Journal of Materials Chemistry B

PAPER

View Article Online
View Journal | View Issue



Cite this: J. Mater. Chem. B, 2016, 4, 7741

# Efficient delivery of chlorin e6 into ovarian cancer cells with octalysine conjugated superparamagnetic iron oxide nanoparticles for effective photodynamic therapy†

Li Zhao,‡[ab] Hongkuan Yang,‡[c] Tsukuru Amano,[d] Hongmei Qin,[b] Luyi Zheng,[d] Akimasa Takahashi,[d] Shiguang Zhao,[e] Ikuo Tooyama,[c] Takashi Murakami[d] and Naoki Komatsu*[b]

Received 7th August 2016,
Accepted 2nd November 2016

DOI: 10.1039/c6tb01988a

www.rsc.org/MaterialsB

In cancer treatment, efficient delivery of active anticancer drugs into cancer cells is highly desirable for maximizing therapeutic effects and alleviating side effects. In this work, a nanocarrier consisting of an $Fe_3O_4$ core, a polyglycerol coating, and an octalysine functionality (SPION-PG-$Lys_8$) has been designed, synthesized and used to deliver a photosensitizer, chlorin e6 (Ce6), into cancer cells for photodynamic therapy (PDT) of cancer cells. SPION-PG-$Lys_8$ is colloidally stable in various aqueous solutions, showing a high positive zeta potential of 47.2 ± 6.9 mV in pure water. *In vitro* characterization reveals that SPION-PG-$Lys_8$ is efficiently taken up by SKOV3 ovarian cancer cells, exhibiting low cytotoxicity, and suppressed autophagy compared to bare SPIONs. Negatively charged Ce6 is thus loaded on the SPION-PG-$Lys_8$ through electrostatic attraction to yield a SPION-PG-$Lys_8$/Ce6 nanocomplex with a positive zeta potential of 22.4 ± 4.3 mV. SPION-PG-$Lys_8$/Ce6 is more easily taken up by the cells than free Ce6, and surprisingly, the internalized SPION-PG-$Lys_8$/Ce6 is found to be enriched in the mitochondria. SPION-PG-$Lys_8$/Ce6 exhibits almost no cytotoxicity under dark conditions, but strong photocytotoxicity due to the light-triggered production of reactive oxygen species (ROS) destroying the mitochondria. Taken together, our results highlight the great potential of SPION-PG-$Lys_8$ as an efficient carrier of Ce6 for photodynamic cancer therapy.

## 1. Introduction

Photodynamic therapy (PDT) uses the combination of a photosensitizer (mainly porphyrin, phthalocyanine or their analogues), oxygen and light to produce cytotoxic reactive oxygen species (ROS) that can kill cancer cells.[1] Different from traditional cancer treatments such as surgery, chemotherapy and radiotherapy, PDT is a non-invasive and region-specific therapy activated solely by light irradiation, thus offering a more targeted treatment and causing minimal impact to normal tissues and organs. In order to enhance PDT efficacy and to alleviate side effects, delivery of active photosensitizers into cancer cells is of crucial importance.[2] Moreover, since ROS have very limited lifetime and diffusion distance,[3] targeting photosensitizers to susceptible parts of cancer cells such as the nucleus and mitochondria is highly desired to trigger cell damage.[4,5]

Emerging nanomedicine has shown that nanoparticles can be used as versatile carriers to effectively deliver photosensitizers to target sites.[6] Furthermore, multi-functionalized nanomedicine is capable of diagnosis, therapy, and monitoring the localization and distribution of therapeutic agents. To date, a variety of nanocarriers such as liposomes,[7] polymeric nanoparticles,[8] and nanocarbons[9] have been developed for the delivery of photosensitizers, which were loaded through either covalent bonding or non-covalent interactions. While the photosensitizer is delivered to tumor sites by these nanocarriers *via* an enhanced permeability and retention (EPR) effect, only very limited amount is taken up by the cancer cells eventually. Thus, it is necessary to explore new nanocarriers to improve the efficiency of the intracellular delivery of photosensitizers.

[a] School of Radiation Medicine and Protection and Collaborative Innovation Center of Radiological Medicine of Jiangsu Higher Education Institutions, Soochow University, Suzhou, Jiangsu 215123, China
[b] Graduate School of Human and Environmental Studies, Kyoto University, Sakyo-ku, Kyoto 606-8501, Japan. E-mail: komatsu.naoki.7w@kyoto-u.ac.jp
[c] Molecular Neuroscience Research Center, Shiga University of Medical Science, Seta Tsukinowa-cho, Otsu, Shiga 520-2192, Japan
[d] Department of Obstetrics and Gynecology, Shiga University of Medical Science, Seta Tsukinowa-cho, Otsu, Shiga 520-2192, Japan
[e] Department of Neurosurgery, 1st Affiliated Hospital, Harbin Medical University, Harbin 150001, China

† Electronic supplementary information (ESI) available. See DOI: 10.1039/c6tb01988a
‡ L. Z. and H. Y. contributed equally to this article.

Superparamagnetic iron oxide nanoparticles (SPIONs) having good biocompatibility are considered as one of the ideal vehicles for the delivery of photosensitizers.[10,11] In particular, SPIONs can be readily engineered through surface modification to impart a variety of functions such as hydrophilicity, fluorescence, specific targeting and drug delivery.[12] On the other hand, cell-penetrating peptides (CPPs) are short peptides rich in cationic arginine- and lysine-residues, which are widely employed for surface modification of nanoparticles to facilitate crossing the cell membranes.[13] Moreover, the CPP conjugation provides nanoparticles with positive charge, enabling complexation with negatively charged genes through electrostatic interaction for gene delivery.[14] In principle, CPP conjugated nanoparticles can also be used for the intracellular delivery of photosensitizers with negative charge, *e.g.*, chlorin e6 (Ce6), a photosensitizer bearing three carboxylic groups.

To prove this concept, in this work we rationally designed octalysine ($Lys_8$) conjugated SPIONs as nanocarriers for the delivery of Ce6 into cancer cells. Specifically, SPIONs were grafted with hydrophilic polyglycerol (PG) through surface-initiated polymerization of glycidol, and the resulting SPION-PG was further surface engineered to conjugate with $Lys_8$ *via* multistep organic transformations and reactions. The obtained SPION-PG-$Lys_8$ possessed excellent colloidal stability in aqueous media as well as positive surface charge. Cellular characterization revealed that SPION-PG-$Lys_8$ showed low toxicity, enhanced cellular uptake, and suppressed autophagy. Ce6 was loaded on SPION-PG-$Lys_8$ through electrostatic attraction and then efficiently delivered into SKOV3 ovarian cancer cells. To our surprise, the internalized Ce6 predominately located in mitochondoria. *In vitro* PDT using the nanophotosensitizer (SPION-PG-$Lys_8$/Ce6) achieved a superior efficacy to free Ce6, highlighting the potential of SPION-PG-$Lys_8$/Ce6 as a promising agent for photodynamic cancer therapy.

## 2. Results and discussion

### 2.1. Preparation and characterization of SPION-PG-$Lys_8$/Ce6

SPION-PG-$Lys_8$/Ce6 was synthesized as shown in Scheme 1. In order to immobilize $Lys_8$, we first synthesized SPION-PG-$N_3$ from SPION-PG through the following functional group transformations: –OH → –OTs (tosylate) → –$N_3$. The resulting

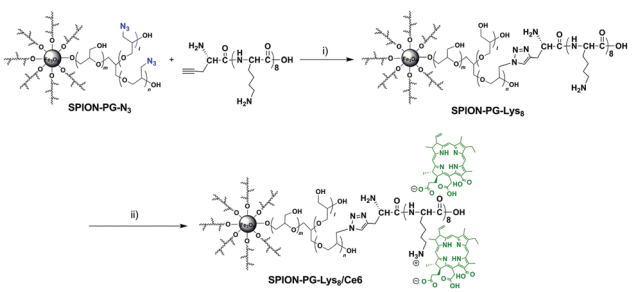


Scheme 1 Synthesis of SPION-PG-$Lys_8$/Ce6 through multi-step organic transformations: (i) copper(II) sulfate pentahydrate, sodium ascorbate, r.t., 96 h; (ii) Ce6, PBS, r.t., 24 h.

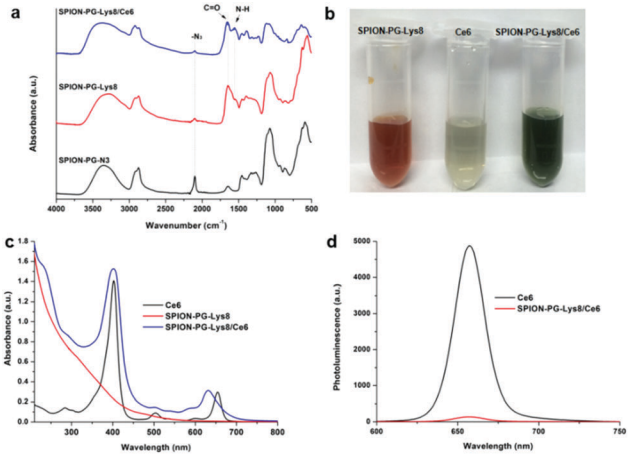


Fig. 1 (a) FTIR spectra of SPION-PG-$N_3$, SPION-PG-$Lys_8$ and SPION-PG-$Lys_8$/Ce6 films; (b) photographs of PBS dispersions of SPION-PG-$Lys_8$, Ce6 and SPION-PG-$Lys_8$/Ce6; (c) UV-Vis absorption spectra of free Ce6, SPION-PG-$Lys_8$ and SPION-PG-$Lys_8$/Ce6 dispersed in PBS; and (d) photoluminescence spectra of free Ce6 and SPION-PG-$Lys_8$/Ce6 dispersed in PBS with the same Ce6 concentration of 0.067 μg $mL^{-1}$. The excitation wavelength is 402 nm.

SPION-PG-$N_3$ was conjugated with alkyne-terminated $Lys_8$ by click chemistry (Scheme 1).[12,14] This was verified by FTIR (Fig. 1a); the azido absorption band of SPION-PG-$N_3$ at 2100 $cm^{-1}$ decreased significantly, and instead two new absorption bands appeared in SPION-PG-$Lys_8$ at 1650 and 1590 $cm^{-1}$, which correspond to the C=O stretching and N–H bending of amide bonds in the peptide, respectively. Due to the superior hydrophilicity of the PG layer and $Lys_8$, the resulting SPION-PG-$Lys_8$ showed very good aqueous dispersibility and stability; the dispersibility in phosphate buffered saline (PBS) is more than 4.0 mg $mL^{-1}$ at 25 °C. Although Ce6 exhibited very poor solubility in pure water and acidic aqueous solutions due to a hydrophobic macrocyclic skeleton, it was readily dissolved in PBS (>1.0 mg $mL^{-1}$ at 25 °C). This is probably because the carboxylic groups (–COOH) at the periphery of Ce6 are more prone to dissociate into carboxylate anions ($–COO^-$) under the slightly basic conditions of PBS (pH = 7.4). To synthesize SPION-PG-$Lys_8$/Ce6, we simply mixed the PBS dispersions of SPION-PG-$Lys_8$ and Ce6, and incubated at room temperature.

The successful loading of Ce6 on SPION-PG-$Lys_8$ was confirmed by the color of the dispersions, UV-Vis absorption and photoluminescence (PL). Fig. 1b shows the photographs of PBS dispersions of SPION-PG-$Lys_8$, Ce6 and SPION-PG-$Lys_8$/Ce6. In contrast to the reddish-brown color of SPION-PG-$Lys_8$, the color of SPION-PG-$Lys_8$/Ce6 changed to dark green, implying the existence of Ce6. Accordingly, the UV-Vis absorption spectrum of SPION-PG-$Lys_8$/Ce6 (Fig. 1c) revealed two new absorption bands with peaks at 402 and 630 nm, which are attributed to the Soret band and Q band of the loaded Ce6, respectively. Compared to those of free Ce6, the broadened Soret band and the blue-shifted Q band of SPION-PG-$Lys_8$/Ce6 support the formation of a (partial) charge-transfer complex. By measuring the absorbance of the Soret band, the Ce6 loading efficiency was quantified to be 7.9 wt%. Fig. 1d shows the PL spectra of

 

Table 1 Hydrodynamic size and zeta potential of SPION derivatives in Milli-Q water

| Sample | Zeta potential [mV] | Hydrodynamic size[a] [nm] |
|---|---|---|
| SPION-PG | −8.4 ± 1.3 | 24.9 ± 5.1 |
| SPION-PG-$Lys_8$ | 47.2 ± 6.9 | 30.5 ± 8.3 |
| SPION-PG-$Lys_8$/Ce6 | 22.4 ± 4.3 | 43.8 ± 15.5 |

[a] Mean diameter ± SD was determined by DLS on the basis of number distribution.

the PBS solution of free Ce6 and the PBS dispersion of SPION-PG-$Lys_8$/Ce6. The emission peaks of both solutions were observed at 658 nm under the excitation of 402 nm, but the fluorescence intensity of SPION-PG-$Lys_8$/Ce6 is much less than that of free Ce6 after normalization of Ce6 concentration owing to the strong fluorescence quenching effect of SPIONs.[15]

To analyze the surface charge of the nanoparticles, we measured the zeta potential of SPION-PG, SPION-PG-$Lys_8$ and SPION-PG-$Lys_8$/Ce6 at neutral pH in Milli-Q water. The results are summarized in Table 1. SPION-PG showed a slight negative zeta potential of −8.4 ± 1.3 mV, whereas the immobilization of $Lys_8$ turned the zeta potential into plus (47.2 ± 6.9 mV for SPION-PG-$Lys_8$) due to the protonation to the amino groups in the peptides. Such a high positive zeta potential enables complexation with negatively charged compounds through electrostatic interaction. Ce6 is considered to possess negative charge in PBS owing to the deprotonation of pendant carboxyl groups. After the complexation of SPION-PG-$Lys_8$ with Ce6, the zeta potential of the resulting SPION-PG-$Lys_8$/Ce6 decreased to 22.4 ± 4.3 mV. The positive surface charge could facilitate the penetration of the nanoparticles into the cell membrane,[16] which will be discussed in detail below.

The particle sizes of SPION-PG-$Lys_8$ and SPION-PG-$Lys_8$/Ce6 in the solid state and in PBS dispersion were characterized by scanning transmission electron microscopy (STEM) and dynamic light scattering (DLS), respectively. As revealed by STEM images (Fig. 2), SPION-PG-$Lys_8$ and SPION-PG-$Lys_8$/Ce6 nanoparticles were individualized on the substrate and exhibited an average core size of about 8 nm, which is consistent with those of SPIONs and SPION-PG. No change in core size indicates that the SPION core is morphologically stable even after the multistep surface engineering. The DLS distributions are shown in the inset of Fig. 2 and the data are summarized in Table 1. The hydrodynamic size of SPION-PG-$Lys_8$ was measured to be 30.5 ± 8.3 nm, which is slightly larger than that of SPION-PG because of the immobilized $Lys_8$ at the periphery. After complexation with Ce6, the hydrodynamic size of SPION-PG-$Lys_8$/Ce6 increased to 43.8 ± 15.5 nm, but no large aggregates more than 100 nm were detected.

It is worth noting that SPION-PG-$Lys_8$/Ce6 possesses high dispersibility in PBS (>1.0 mg $mL^{-1}$) as well as excellent colloidal stability. Only a few precipitates were found at the bottom after standing at room temperature for 4 weeks, and the precipitates can be readily redispersed by mild bath sonication. Little change in hydrodynamic size was detected in water over this period as measured by DLS, implying little release of Ce6. Actually, almost no free Ce6 was detected in the aqueous dispersions of SPION-PG-$Lys_8$/Ce6 under neutral to acidic conditions (pH = 4.0, 6.9 and 7.4) after incubation at 37 °C for 96 h (Fig. S1, ESI†). On the other hand, Ce6 was gradually dissociated from SPION-PG-$Lys_8$/Ce6 under basic conditions (pH 9.2).

### 2.2. Cytotoxicity, cell uptake, and subcellular localization

Since biocompatibility is a prerequisite for nanoparticles as drug delivery carriers, the effect of SPION-PG-$Lys_8$ on the viability of NIH3T3 mouse fibroblast cells and SKOV3 human ovarian adenocarcinoma cells was investigated by the CCK-8 assay. SPION-PG-$Lys_8$ exhibited no significant cytotoxicity to NIH3T3 cells at concentrations up to 100 μg $mL^{-1}$ and slight cytotoxicity to SKOV3 cells only at 100 μg $mL^{-1}$ after incubation with the cells for 24, 48, and 72 h (Fig. 3). These results indicate that SPION-PG-$Lys_8$ is a biocompatible candidate as a drug carrier. Cytotoxicity of SPION-PG-$Lys_8$/Ce6 with or without light irradiation will be evaluated in Fig. 9.

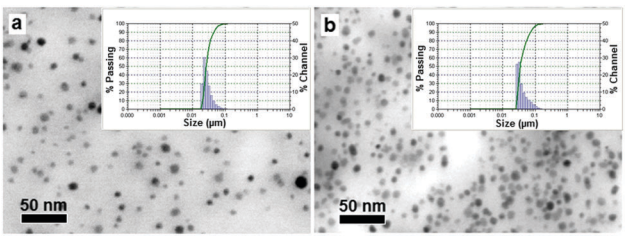


Fig. 2 STEM images of (a) SPION-PG-$Lys_8$ and (b) SPION-PG-$Lys_8$/Ce6. Insets are DLS distributions (number) of the nanoparticles in PBS.

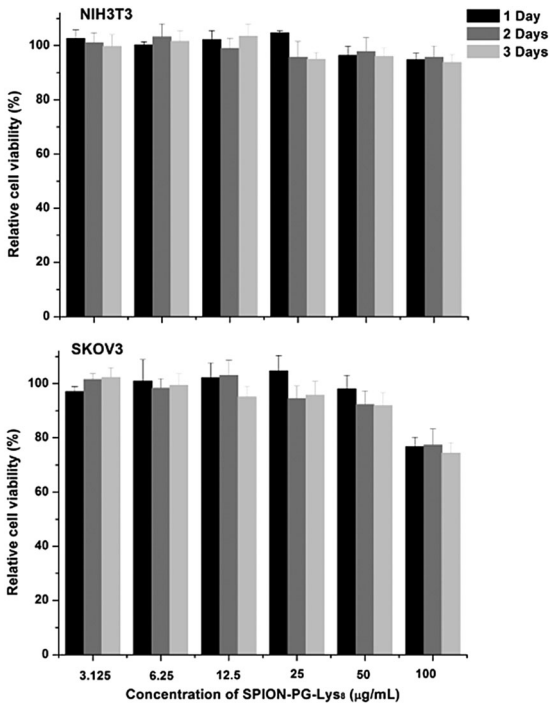


Fig. 3 Cell viability of NIH3T3 cells and SKOV3 cells treated with SPION-PG-$Lys_8$ at different concentrations for 24, 48, and 72 h ($n$ = 3, mean ± SD).

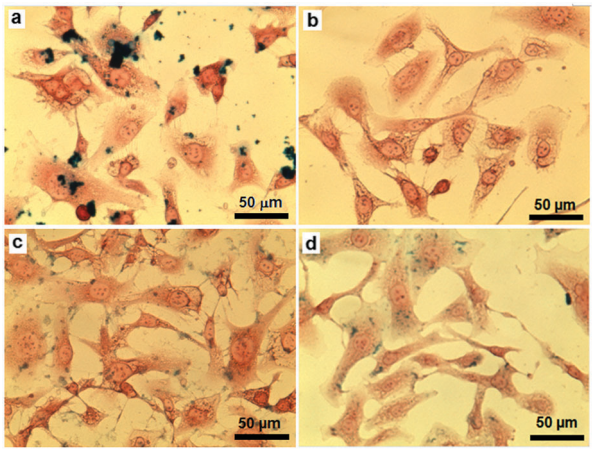


Fig. 4 Prussian blue staining of SKOV3 cells treated with SPION-based nanoparticles for 24 h: (a) pristine SPION, 10 μg mL$^{-1}$; (b) SPION-PG, 100 μg mL$^{-1}$; (c) SPION-PG-Lys$_8$, 10 μg mL$^{-1}$; and (d) SPION-PG-Lys$_8$/Ce6, 10 μg mL$^{-1}$.

In order to study the cellular uptake of the SPION-based nanoparticles, SKOV3 cells treated with pristine SPIONs, SPION-PG, SPION-PG-Lys$_8$ and SPION-PG-Lys$_8$/Ce6 for 24 h were stained with Prussian blue and the resulting images are shown in Fig. 4. As pristine SPIONs have very poor aqueous dispersibility, they easily aggregated and precipitated immediately after being added to the cell culture medium. As a consequence, a lot of pristine SPION aggregates were found in the cells due to endocytosis. In contrast, SPION-PG was not internalized even at a high concentration of 100 μg mL$^{-1}$, which is consistent with our previous observations in other cancer cells.[12] These results indicate that grafted PG is capable of shielding nanoparticles from cell uptake. In the cases of SPION-PG-Lys$_8$ and SPION-PG-Lys$_8$/Ce6, both nanoparticles were clearly stained in SKOV3 cells by virtue of cell-penetrating Lys$_8$ as well as their positive surface charge.[17]

Taking advantage of the red fluorescence of Ce6, the cell uptake of Ce6 and SPION-PG-Lys$_8$/Ce6 was compared by confocal laser scanning microscopy (CLSM). As shown in Fig. 5a, the SKOV3 cells incubated at a Ce6 concentration of 4.0 μg mL$^{-1}$ displayed very dim red fluorescence (Cy5), indicating low cell uptake of Ce6. This is probably because the negative charge of Ce6 inhibits binding to cell membranes which also have a negative charge. In sharp contrast, bright red fluorescence was

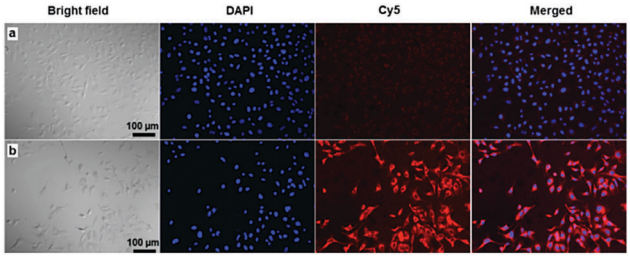


Fig. 5 Confocal fluorescence images of SKOV3 cells treated with (a) free Ce6 and (b) SPION-PG-Lys$_8$/Ce6 for 8 h at the same Ce6 concentration of 4.0 μg mL$^{-1}$.

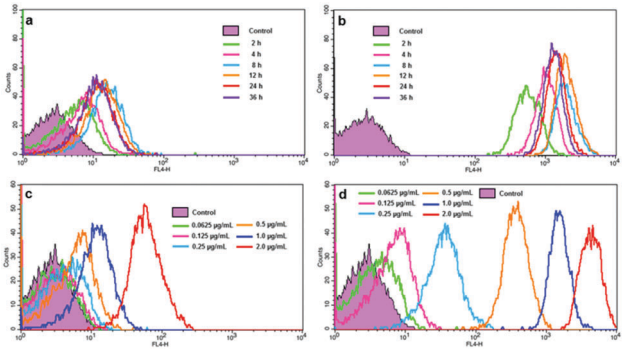


Fig. 6 FACS analysis of SKOV3 cells treated with (a) Ce6 and (b) SPION-PG-Lys$_8$/Ce6 at the Ce6 concentration of 1.0 μg mL$^{-1}$ for different incubation periods (2–36 h), and (c) Ce6 and (d) SPION-PG-Lys$_8$/Ce6 at different Ce6 concentrations (0.0625–2.0 μg mL$^{-1}$) for 12 h.

detected in the cytoplasm of SKOV3 cells treated with SPION-PG-Lys$_8$/Ce6 at the same Ce6 concentration (Cy5 in Fig. 5b). Taking the strong fluorescence quenching effect of SPIONs into account, the amount of internalized Ce6 carried by SPION-PG-Lys$_8$ should be much larger than that of Ce6 without a carrier.

We further studied the cell uptake profiles of Ce6 and SPION-PG-Lys$_8$/Ce6 by flow cytometry (FACS). The cell uptake of Ce6 is found to be facilitated significantly with the carrier, as the fluorescence intensity in Fig. 6b and d is compared with that in Fig. 6a and c, respectively. With 12 h incubation, the cellular fluorescence intensity of SKOV3 cells treated with SPION-PG-Lys$_8$/Ce6 (Fig. 6d) is several hundred times stronger than that of Ce6 treated cells (Fig. 6c). This is in good agreement with the aforementioned observations using fluorescence microscopy (Fig. 5). The fluorescence intensity is also found to depend on both Ce6 concentration and incubation time. When SKOV3 cells were incubated with Ce6 or SPION-PG-Lys$_8$/Ce6 at different Ce6 concentrations from 0.0625 to 2.0 μg mL$^{-1}$ for 12 h, the cellular fluorescence intensity increases according to the increase of Ce6 concentration as shown in Fig. 6c and d. The cellular fluorescence intensity of SKOV3 cells treated with either Ce6 or SPION-PG-Lys$_8$/Ce6 (Ce6 concentration of 1.0 μg mL$^{-1}$) also changed with incubation time; increased at 2–4 h, maximum at 8–12 h, and slightly decreased at 24–36 h (Fig. 6a and b).

Based on the efficient cell uptake of SPION-PG-Lys$_8$/Ce6, its subcellular distribution in SKOV3 cells was next investigated by CLSM (Fig. 7). While lysosome is commonly indicated as a major intracellular depositing site for internalized nanoparticles,[18–20] it has been reported that the nanoparticles possessing positive charge and lipophilicity tend to localize in mitochondria rather than lysosomes.[21–23] In the case of SPION-PG-Lys$_8$/Ce6, positive charge and lipophilicity are provided by Lys$_8$ and Ce6, respectively. This indicates that SPION-PG-Lys$_8$/Ce6 might also have mitochondria-targeting capability. As shown in Fig. 7d and e, internalized SPION-PG-Lys$_8$/Ce6 signal (shown in red) mainly colocalized with mitochondria labeled by transient transfection of a DsRed2-Mito plasmid (shown in blue). In addition, lysosomes stained by LysoTracker (shown in green) rarely

 

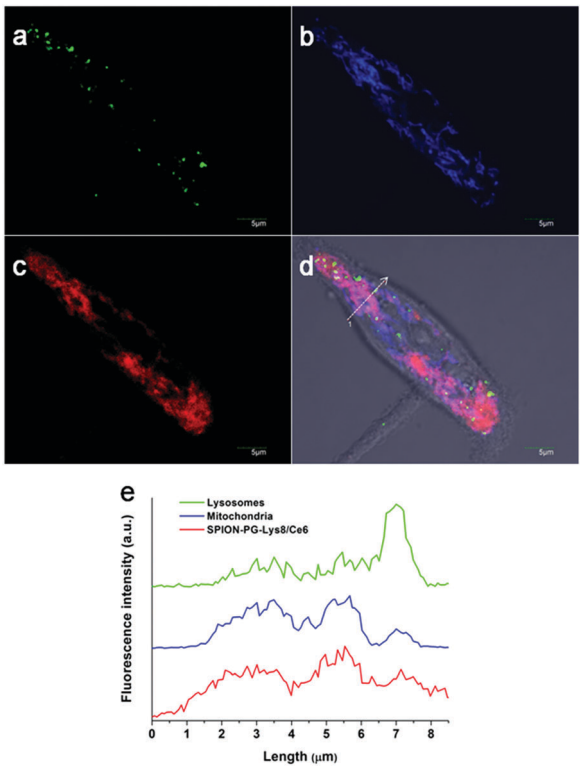


Fig. 7 Subcellular localization of internalized SPION-PG-Lys$_8$/Ce6 in SKOV3 cells. (a) Lysosomes (green); (b) mitochondria in DsRed2-mito expressing cells (blue); (c) subcellular distribution of SPION-PG-Lys$_8$/Ce6 (red); (d) merged images; and (e) fluorescence intensity profile across the arrowed line shown in (d).

colocalized with either SPION-PG-Lys$_8$/Ce6 or mitochondria. These observations suggest that internalized SPION-PG-Lys$_8$/Ce6 tends to localize in mitochondria, but not in lysosomes.

### 2.3. Assay of autophagy induced by nanocarriers

A growing body of literature suggests that nanoparticles are involved in autophagy perturbation, and autophagy may serve as a self-protective mechanism by degrading foreign particles, damaged organelles and proteins.[24] Thus, inhibition of autophagy usually sensitizes the anticancer therapy of nanomaterials.[25] To explore whether SPION-PG-Lys$_8$ affects autophagy, LC3-II as an autophagy marker was detected by a western blot, since the amount of LC3-II is associated with the number of autophagosomes, which engulf cytoplasmic components into lysosomes during autophagy. The western blot (Fig. 8a) shows two bands recognized by anti-LC3 antibody: LC3-I (upper band) and LC3-II (lower band). The amount of LC3-II normalized to a loading control is considered as an emerging consensus to evaluate the autophagy[26,27] and was expressed as the ratio of LC3-II to β-actin. Quantitative graph in Fig. 8a shows a significant increase of LC3-II/β-actin in cells treated with SPIONs (40 μg mL$^{-1}$) compared to untreated cells, which is consistent with previous reports that iron oxide nanoparticles induce autophagy in cancer cells.[28,29] Interestingly, compared to SPIONs, SPION-PG-Lys$_8$ at the same concentration showed less LC3-II/β-actin, indicating a suppressed autophagy. This result is supported by the confocal

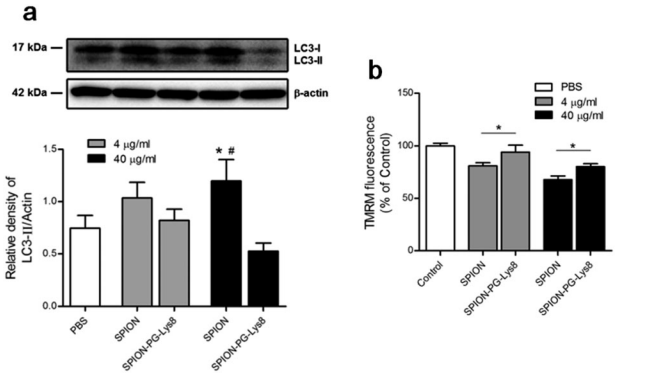


Fig. 8 (a) Autophagy marker, LC3 induced by SPION and SPION-PG-Lys$_8$. SKOV3 cells were treated with SPION and SPION-PG-Lys$_8$ at the indicated concentrations, and LC3 and β-actin levels were determined by a western blot. Protein levels were semi-quantified by calculating band densities and expressed as the ratio of LC3-II to β-actin shown in the quantitative graph ($n$ = 3, mean ± SD, *$p$ < 0.05 *versus* the untreated, #$p$ < 0.05 *versus* 40 μg mL$^{-1}$ SPION-PG-Lys$_8$); (b) MMP detection by TMRM staining ($n$ = 3, mean ± SD, *$p$ < 0.05).

images where lysosomes are colocalized with neither nanoparticles nor mitochondria (Fig. 7), implying that SPION-PG-Lys$_8$ does not tend to be transferred to lysosomes for degradation *via* the autophagy process. Furthermore, the loss of mitochondrial membrane potential (MMP) triggers mitochondrial autophagy (mitophagy)[30,31] which may therefore degrade mitochondria-localized nanoparticles. Therefore, we further determined MMP levels with TMRM staining (Fig. 8b). The result shows that MMP levels are slightly reduced in SPION-treated SKOV3 cells at concentrations of 4.0 μg mL$^{-1}$ and 40 μg mL$^{-1}$, compared with those in the cells treated with SPION-PG-Lys$_8$, implying that SPION-PG-Lys$_8$ does not tend to induce mitophagy by impairing MMP in comparison with SPIONs. Accordingly, the CCK-8 assay (Fig. S2, ESI†) showed that autophagy inhibition by bafilomycin A1 (Baf) or chloroquine (CQ) does not alter SPION-PG-Lys$_8$/Ce6-induced cell death, suggesting that autophagy may not play a vital role in the efficacy of SPION-PG-Lys$_8$/Ce6.

Moreover, nanomaterial-induced autophagy is commonly triggered by nanomaterial-induced oxidative stress,[32–34] and iron oxide nanoparticles are reported to generate increased ROS production which is correlated with autophagy.[28,35] However, our data show that SPION-PG-Lys$_8$ does not cause a significant increase of ROS production by analyzing $H_2$DCFDA with

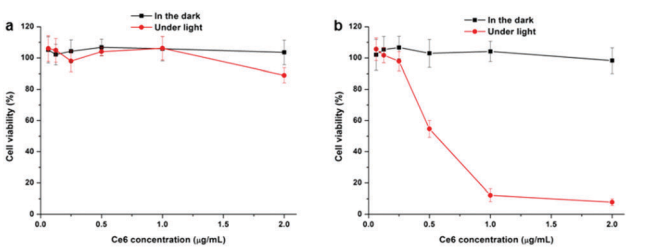


Fig. 9 CCK-8 assay of SKOV3 cells treated with (a) Ce6 and (b) SPION-PG-Lys$_8$/Ce6 at different Ce6 concentrations in the dark and under light irradiation (16.8 J cm$^{-2}$) ($n$ = 3, mean ± SD).

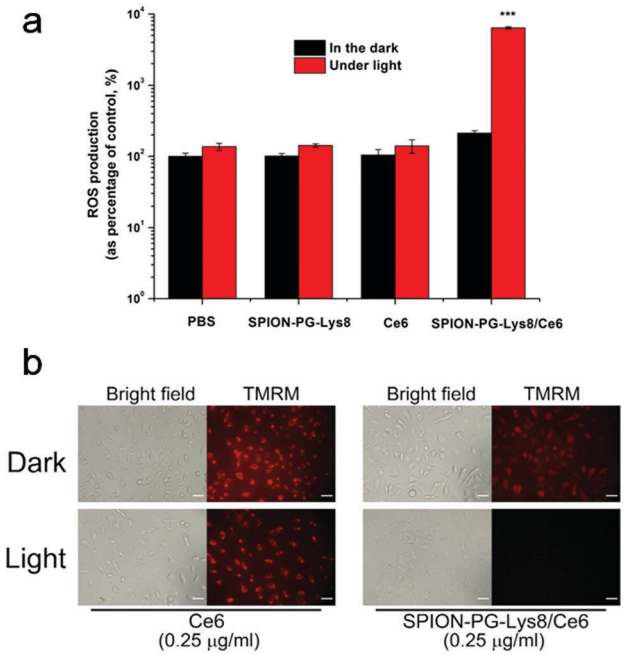


Fig. 10 (a) ROS levels in SKOV3 cells after treatment with PBS (10% v/v), SPION-PG-$Lys_8$ (2.5 μg $mL^{-1}$), Ce6 (0.25 μg $mL^{-1}$) and SPION-PG-$Lys_8$/Ce6 (0.25 μg Ce6 per mL) for 24 h. The cells treated with PBS in the dark are used as a control ($n$ = 3, mean ± SD, ***$p < 0.001$); (b) MMP assay of SKOV3 cells after treatment with Ce6 (0.25 μg $mL^{-1}$) and SPION-PG-$Lys_8$/Ce6 (0.25 μg Ce6 per mL) for 24 h. Bright field and TMRM images were obtained using a fluorescence microscope. Scale bar = 200 μm.

flow cytometry (*vide infra*, Fig. 10a). This might account for the lower level of autophagy induced by SPION-PG-$Lys_8$ compared to that induced by SPIONs. Although it has been suggested that a wide range of nanomaterials induce or inhibit autophagy,[24] it is not yet reported how cationic iron oxide nanoparticles (SPION-PG-$Lys_8$) affect autophagy. Further experiments are needed to explore whether positively charged iron oxide plays a role in inhibiting autophagy.

### 2.4. *In vitro* cytotoxicity assay and intracellular ROS detection

*In vitro* cytotoxicity of Ce6 and SPION-PG-$Lys_8$/Ce6 was evaluated by the CCK-8 assay and the results are shown in Fig. 9. Under dark conditions, both photosensitizers showed negligible influence on the viability of SKOV3 cells, indicating no or very low cytotoxicity of these materials themselves. Under irradiation of 660 nm light (16.8 J $cm^{-2}$), the Ce6 treated SKOV3 cells showed slightly lower viability only at the highest applied dosage of 2.0 μg $mL^{-1}$ and the nanocarrier, SPION-PG-$Lys_8$, exhibited almost no cytotoxicity up to the concentration of 50 μg $mL^{-1}$ (Fig. S3, ESI†). In contrast, SPION-PG-$Lys_8$/Ce6 exhibited remarkable and concentration-dependent photocytotoxicity. This result combined with the cell uptake assay suggests that *in vitro* PDT efficacy is proportional to the amount of Ce6 internalized into the cells.

To gain more insight into the enhanced PDT of the SPION-PG-$Lys_8$/Ce6, we quantified intracellular ROS levels by FACS using H2DCFDA as a fluorescent indicator. As shown in Fig. 10a, similar ROS levels with respect to control were detected from the SKOV3 cells treated with SPION-PG-$Lys_8$ and Ce6 both in the dark and under light irradiation. Since ROS generation was confirmed in a Ce6 solution with the same concentration (0.25 μg $mL^{-1}$) under light irradiation without cells (Fig. S4, ESI†), the Ce6 applied to the SKOV3 cells is concluded not to be taken up by the cells and to be washed out before light irradiation. For SPION-PG-$Lys_8$/Ce6 shown in Fig. 10a, the ROS production rose sharply by about 300 times under light irradiation, whereas it was slightly higher than the normal level in the dark. In addition, it was confirmed that a solution of SPION-PG-$Lys_8$/Ce6 (0.25 μg Ce6 per mL) in the absence of cells generated ROS under light irradiation (Fig. S4, ESI†), while almost no ROS was detected in SPION-PG-$Lys_8$ solution. These results suggest that Ce6 was carried in the cells by SPION-PG-$Lys_8$ and ROS was produced in the cells under light irradiation. The result was also verified using confocal fluorescence microscopy (Fig. S5, ESI†). Considering that SPION-PG-$Lys_8$/Ce6 is enriched in the mitochondria, the induced oxidative stress can cause mitochondrial dysfunctions or disruptions, which would be one of the major reasons for eventual cell apoptosis. To verify this speculation, the MMP level of the treated cells was characterized and the results are shown in Fig. 10b. An almost complete loss of TMRM fluorescence was observed in light exposed cells treated with SPION-PG-$Lys_8$/Ce6, suggesting a dramatic decrease in MMP caused by light-triggered ROS.

Finally, we evaluated the photostability of Ce6 (0.25 μg $mL^{-1}$) and SPION-PG-$Lys_8$/Ce6 (0.25 μg Ce6 per mL) in PBS. After photoirradiation of 660 nm light (141 mW $cm^{-2}$) for different periods of time (0.5, 1, 2, 4, 8, and 16 min), the absorbance at the Soret band (402 nm) was monitored (Fig. 11). When Ce6 is not loaded on the carrier, Ce6 is unstable against photoirradiation; that is, more than 70% of Ce6 was degraded in a few minutes. In sharp contrast, almost no degradation of Ce6 was observed in SPION-PG-$Lys_8$/Ce6. These results indicate the dual role of the nanocarrier, SPION-PG-$Lys_8$, for the cytotoxic effect (Fig. 9) or

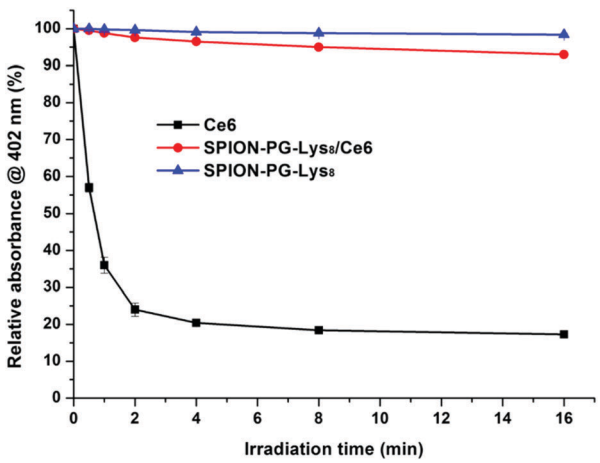


Fig. 11 Photostability of Ce6, SPION-PG-$Lys_8$ and SPION-PG-$Lys_8$/Ce6 after irradiation with 660 nm light (141 mW $cm^{-2}$) for different periods of time (0.5, 1, 2, 4, 8, and 16 min). The relative absorbance at 402 nm (%) is calculated according to the equation, $A_{\text{after irradiation}}/A_{\text{before irradiation}} \times 100$.

ROS generation (Fig. 10), to deliver Ce6 into the cells and to protect Ce6 from degradation under light irradiation.

# 3. Experimental

### Materials and instruments

All the reagents and solvents used for the synthesis were employed as received. SPIONs were prepared by the polyol method and surface engineered according to our recent report. Octalysine that binds propargyl glycine (G*) at an N terminal (G*$Lys_8$) was synthesized by the Central Research Laboratory of the Shiga University of Medical Science. Ce6 was purchased from MedKoo Biosciences. Dialysis was carried out using a Spectra/Pro® dialysis membrane, MWCO: 12–14 kDa.

UV-Vis absorption measurements were carried out using a Shimadzu UV-3100PC spectrophotometer. Photoluminescence was conducted on a Hitachi F-4500 fluorescence spectrophotometer. FTIR spectral measurements were conducted using an IR Prestige-21 (Shimadzu Co.). The pellet consisting of the sample and KBr was recorded in transmittance mode. Hydrodynamic diameters in solution were determined by dynamic light scattering (DLS) using a Nanotrac UPA-UT151 system (Microtrac, Inc.). Scanning transmission electron microscopy (STEM) was performed on a JEOL JSM-7500F field emission scanning electron microscope at an accelerating voltage of 25 kV for the TEM model. All samples for electron microscopy were prepared by evaporating one drop ($\sim$50 μL) of samples on ultrathin carbon-coated copper grids. Zeta potential measurement was conducted in water dispersions using a Malvern Zetasizer Nano ZS.

### Synthesis of SPION-PG-$Lys_8$

The click reaction of SPION-PG-$N_3$ and G*$Lys_8$ was conducted in a similar manner to our reported procedure.[14] G*$Lys_8$ (4.0 mg) in water (1.0 mL) was added to a dispersion of SPION-PG-$N_3$ (20 mg) in water (4.0 mL). Copper(II) sulfate pentahydrate (12 mg) in water (0.5 mL) and sodium ascorbate (10 mg) in water (0.5 mL) were added to the mixture with vigorous stirring. The resulting brown suspension was bath sonicated for 10 min and stirred at room temperature for 96 h. Insoluble copper salts were removed by centrifugation (Kubota 3700) at 1000 rpm for 5 min and the supernatant including the product was further purified by rinsing with 1% ammonia and water using a centrifugal filter (Amicon® Ultra-15, MWCO: 100 K). It was characterized by FTIR (Fig. 1a).

### Synthesis of SPION-PG-$Lys_8$/Ce6

To a PBS dispersion of SPION-PG-$Lys_8$ (2.0 mg $mL^{-1}$, 5.0 mL) a PBS solution of Ce6 (1.0 mg $mL^{-1}$, 2.0 mL) was added. The mixture was stirred at room temperature in the absence of light for 24 h. The product was purified by rinsing repeatedly with PBS using the centrifugal filter and then redispersed in PBS by mild bath sonication. For cell experiments, the dispersion was further sterilized by passing through a syringe-driven filter (MILLEX®GP, 0.22 μm).

# 4. Conclusions

In summary, multifunctional $Lys_8$ moieties were covalently grafted on the periphery of SPION-PG through rational surface engineering for use as nanocarriers for drug delivery. The designed SPION-PG-$Lys_8$ showed excellent dispersibility and stability in aqueous solutions, as well as low cytotoxicity. In particular, SPION-PG-$Lys_8$ demonstrated a suppressed autophagy compared to bare SPIONs, benefiting cancer drug therapy. The positively charged $Lys_8$ not only enabled loading of Ce6 through electrostatic attraction, but also facilitated a more efficient uptake of the resulting SPION-PG-$Lys_8$/Ce6 by SKOV3 cancer cells than free Ce6. Moreover, the internalized SPION-PG-$Lys_8$/Ce6 was found to be predominately localized in mitochondria, resulting in strong photocytotoxicity to the cells due to the effective destruction of the mitochondria by light-triggered ROS produced. The results highlight the great potential of SPION-PG-$Lys_8$ as an efficient carrier of Ce6 for photodynamic cancer therapy. We envision that SPION-PG-$Lys_8$ may be further used in the delivery of more negatively charged drugs and genes as well as diagnosis in magnetic resonance imaging (MRI) as a theranostic agent.

# Acknowledgements

The authors thank Dr Y. Niwa (Shiga University of Medical Science) for technical support with cell experiments and Mr J. Xu (Kyoto University) for assistance with zeta potential measurement. This work was partially supported by the Naito Foundation (N. K.), the Natural Science Foundation of Jiangsu Province (BK20160329) and the Natural Science Foundation of China (31600805) (L. Z.).

# Notes and references

1 D. E. Dolmans, D. Fukumura and R. K. Jain, *Nat. Rev. Cancer*, 2003, **3**, 380–387.
2 Z. Zhen, W. Tang, W. Zhang and J. Xie, *Nanoscale*, 2015, **7**, 10330–10333.
3 X. Wang, H. Fang, Z. Huang, W. Shang, T. Hou, A. Cheng and H. Cheng, *J. Mol. Med.*, 2013, **91**, 917–927.
4 S. Fulda, L. Galluzzi and G. Kroemer, *Nat. Rev. Drug Discovery*, 2010, **9**, 447–464.
5 X. Li, P. Fang, J. Mai, E. T. Choi, H. Wang and X.-F. Yang, *J. Hematol. Oncol.*, 2013, **6**, 1–19.
6 S. S. Lucky, K. C. Soo and Y. Zhang, *Chem. Rev.*, 2015, **115**, 1990–2042.
7 A. S. L. Derycke and P. A. M. de Witte, *Adv. Drug Delivery Rev.*, 2004, **56**, 17–30.
8 H. Kim, S. Mun and Y. Choi, *J. Mater. Chem. B*, 2013, **1**, 429–431.
9 G. Liu, H. Qin, T. Amano, T. Murakami and N. Komatsu, *ACS Appl. Mater. Interfaces*, 2015, **7**, 23402–23406.
10 H. Gu, K. Xu, Z. Yang, C. K. Chang and B. Xu, *Chem. Commun.*, 2005, 4270–4272.
11 Z. Li, C. Wang, L. Cheng, H. Gong, S. Yin, Q. Gong, Y. Li and Z. Liu, *Biomaterials*, 2013, **34**, 9160–9170.

12 L. Zhao, T. Chano, S. Morikawa, Y. Saito, A. Shiino, S. Shimizu, T. Maeda, T. Irie, S. Aonuma and H. Okabe, *Adv. Funct. Mater.*, 2012, **22**, 5107–5117.
13 S. M. Farkhani, A. Valizadeh, H. Karami, S. Mohammadi, N. Sohrabi and F. Badrzadeh, *Peptides*, 2014, **57**, 78–94.
14 L. Zhao, Y. Nakae, H. Qin, T. Ito, T. Kimura, H. Kojima, L. Chan and N. Komatsu, *Beilstein J. Org. Chem.*, 2014, **10**, 707–713.
15 Y. Hou, J. Zhou, Z. Gao, X. Sun, C. Liu, D. Shangguan, W. Yang and M. Gao, *ACS Nano*, 2015, **9**, 3199–3205.
16 C. Loos, T. Syrovets, A. Musyanovych, V. Mailänder, K. Landfester, G. U. Nienhaus and T. Simmet, *Beilstein J. Nanotechnol.*, 2014, **5**, 2403–2412.
17 A. El-Sayed, I. A. Khalil, K. Kogure, S. Futaki and H. Harashima, *J. Biochem.*, 2008, **283**, 23450–23461.
18 S. Manchun, C. R. Dass and P. Sriamornsak, *Life Sci.*, 2012, **90**, 381–387.
19 L. Zhao, Y. H. Xu, H. Qin, S. Abe, T. Akasaka, T. Chano, F. Watari, T. Kimura, N. Komatsu and X. Chen, *Adv. Funct. Mater.*, 2014, **24**, 5348–5357.
20 L. Zhao, Y.-H. Xu, T. Akasaka, S. Abe, N. Komatsu, F. Watari and X. Chen, *Biomaterials*, 2014, **35**, 5393–5406.
21 R. A. Smith, C. M. Porteous, A. M. Gane and M. P. Murphy, *Proc. Natl. Acad. Sci. U. S. A.*, 2003, **100**, 5407–5412.
22 S. Marrache and S. Dhar, *Proc. Natl. Acad. Sci. U. S. A.*, 2012, **109**, 16288–16293.
23 Q. Qu, X. Ma and Y. Zhao, *Nanoscale*, 2015, **7**, 16677–16686.
24 S. T. Stern, P. P. Adiseshaiah and R. M. Crist, *Part. Fibre Toxicol.*, 2012, **9**, 1.
25 E. Panzarini, V. Inguscio, B. A. Tenuzzo, E. Carata and L. Dini, *Cancers*, 2013, **5**, 296–319.
26 G. Chen, Z. Ke, M. Xu, M. Liao, X. Wang, Y. Qi, T. Zhang, J. A. Frank, K. A. Bower and X. Shi, *Autophagy*, 2012, **8**, 1577–1589.
27 S. Barth, D. Glick and K. F. Macleod, *J. Pathol.*, 2010, **221**, 117–124.
28 J. Lin, Z. Huang, H. Wu, W. Zhou, P. Jin, P. Wei, Y. Zhang, F. Zheng, J. Zhang and J. Xu, *Autophagy*, 2014, **10**, 2006–2020.
29 M. I. Khan, A. Mohammad, G. Patil, S. Naqvi, L. Chauhan and I. Ahmad, *Biomaterials*, 2012, **33**, 1477–1488.
30 M. Priault, B. Salin, J. Schaeffer, F. Vallette, J. Di Rago and J. Martinou, *Cell Death Differ.*, 2005, **12**, 1613–1621.
31 G. Twig, A. Elorza, A. J. Molina, H. Mohamed, J. D. Wikstrom, G. Walzer, L. Stiles, S. E. Haigh, S. Katz and G. Las, *EMBO J.*, 2008, **27**, 433–446.
32 N. Li, T. Xia and A. E. Nel, *Free Radicals Biol. Med.*, 2008, **44**, 1689–1699.
33 M. Narita, A. R. Young, S. Arakawa, S. A. Samarajiwa, T. Nakashima, S. Yoshida, S. Hong, L. S. Berry, S. Reichelt and M. Ferreira, *Science*, 2011, **332**, 966–970.
34 Q. Zhang, W. Yang, N. Man, F. Zheng, Y. Shen, K. Sun, Y. Li and L.-P. Wen, *Autophagy*, 2009, **5**, 1107–1117.
35 E.-J. Park, D.-H. Choi, Y. Kim, E.-W. Lee, J. Song, M.-H. Cho, J.-H. Kim and S.-W. Kim, *Toxicol. In Vitro*, 2014, **28**, 1402–1412.

 